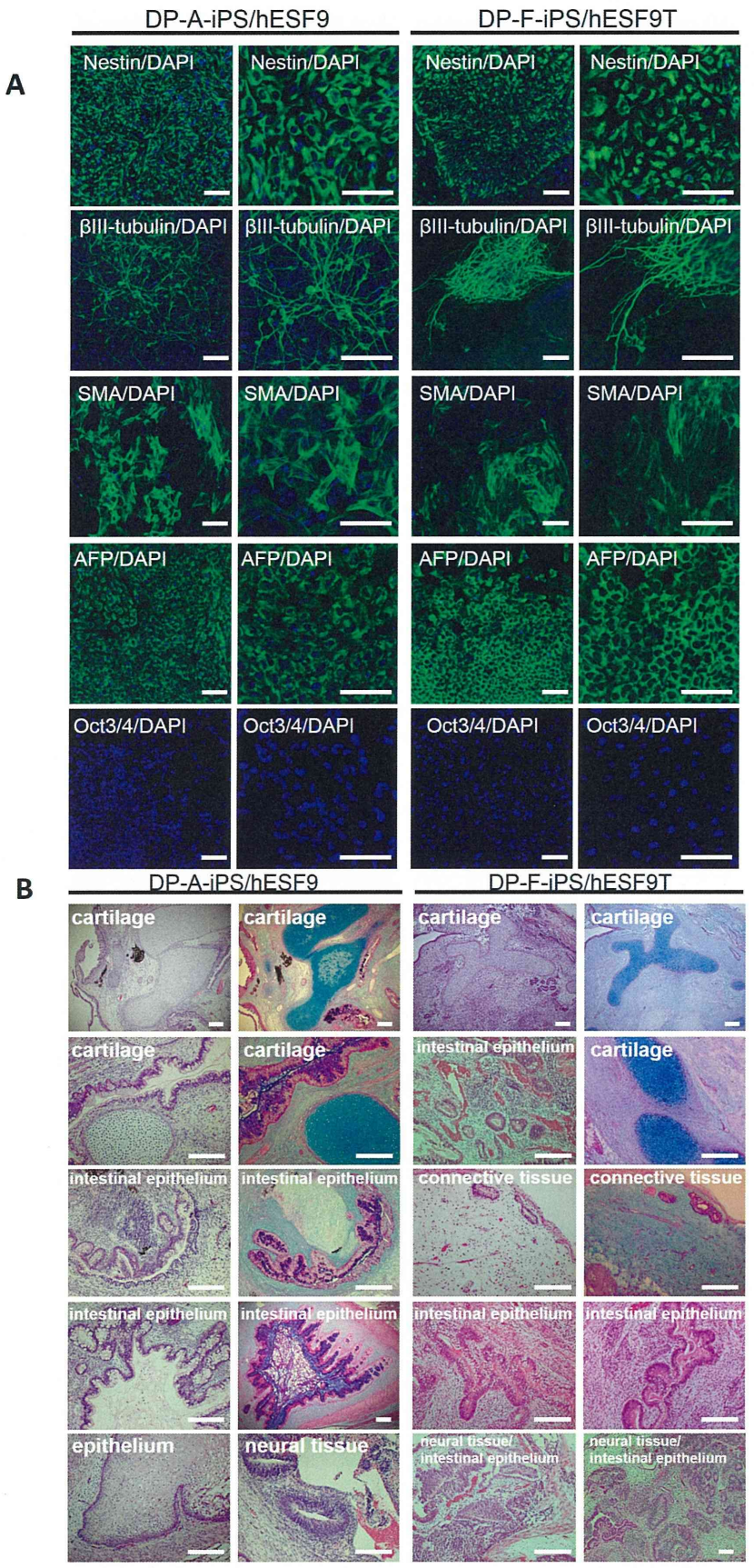
A
DP-A-iPS/hESF9
DP-F-iPS/hESF9T
Nestin/DAPI
βIII-tubulin/DAPI
SMA/DAPI
AFP/DAPI
Oct3/4/DAPI
B
DP-A-iPS/hESF9
DP-F-iPS/hESF9T
cartilage
intestinal epithelium
connective tissue
epithelium
neural tissue
neural tissue/
intestinal epithelium

Figure 6. Embryoid body-mediated differentiation of hiPSCs derived from DPCs in serum-free and feeder-free defined culture conditions and teratoma formation of hiPSCs in the defined culture conditions. A) Differentiation was performed using embryoid body formation, and the differentiated iPSCs (DP-A-iPS/hESF9 or DP-F-iPS/hESF9T) were fixed and reacted with antibodies. Shown were immunocytochemistry of Nestin, βIII-tubulin, α-smooth muscle actin (α-SMA), and α-fetoprotein (AFP). Binding of these antibodies was visualized with Alexa Fluor 488-conjugated secondary antibodies (green). Oct3/4 was also investigated. Binding of these antibodies was visualized with Alexa Fluor® 594-conjugated secondary antibodies (red). Nucleuses were stained with DAPI. (passage 25). Bar indicates 100 μm. B) Teratomas were generated in SCID mice (CB17/Icr-*Prkdc*^{scid}/CrlCrlj) from DP-A-iPS and DP-F-iPS grown under hESF9 or hESF9T-based conditions. Histological analysis with HE staining or Alcian Blue staining demonstrated that teratomas formed from iPS cells cultured in KSR-based (data not shown) or in hESF9T-based conditions contained derivatives of all three germ layers. Left panel shows teratomas from DP-A-iPS-CL1 at passage 22. Right panel shows teratomas from DP-F-iPS-CL14 at passage 6. Scale bars represent 200 μm.
doi:10.1371/journal.pone.0087151.g006

self-renewal, cell death, and cell differentiation, and it supports substantially improved reprogramming efficiencies. Although we have only demonstrated improved efficiencies for viral-based reprogramming, these conditions should be equally useful for other non-integrative reprogramming approaches [33–40]. Finally, since hESF9T medium is defined, it should also help facilitate the transfer of basic research on human pluripotent stem cells to the clinic and useful for understanding disease mechanisms, drug screening, and toxicology.

Conclusions

We have successfully generated hiPSCs from adult human dental pulp cells (DPCs) and maintained them in an undifferentiated state in serum-free defined medium. Furthermore these generated hiPSCs continued to proliferate and retained the properties of self-renewal and pluripotency for a prolonged period of time in the presence of appropriate amount of TGF-β1. As a result, we found TGF-β1 to be an important factor in maintaining pluripotency of hiPSCs. As this simple serum-free adherent monoculture system allows us to elucidate cellular responses to growth factors under defined conditions, these advantages will help to clarify the molecular mechanisms at play in early development.

Supporting Information

Figure S1 Transduction Efficiency of Retroviruses in TIG-3. TIG-3 was introduced with pMXs retroviruses containing the EGFP cDNA. After 4 days, cells were photographed under a fluorescence microscope and analyzed by flow cytometry. The upper panel shows the images of phase contrast and fluorescent microscope. The lower panel shows the result of flow cytometry. Shown are percentages of cells expressing EGFP.
(TIF)

Figure S2 Morphology of transduced TIG-3 on each ECMs in hESF9 medium. A) Upper figures: Twenty days after transduction TIG-3-derived human iPS colony were picked up and sub-cultured on each ECMs. Lower figures: Images of sub-cultured iPS colonies seeded on each ECMs with hESF9 medium for the indicated days at the left. B) Expression of ES cell marker genes in iPSCs derived from TIG-3 cultured on each ECMs with hESF9 medium at day 4. The expression of pluripotency marker genes; Nanog were weakened or disappeared when picked up and sub-cultured on collagen and gelatin. We used primers that only amplified the endogenous genes. #1: hiPSCs generated from TIG-3 on gelatin-coated dish and sub-cultured on gelatin-coated dishes with hESF9 medium at passage 2. #2: hiPSCs generated from TIG-3 on collagen-coated dish and sub-cultured on collagen-coated dishes with hESF9 medium at passage 2. #3: hiPSCs generated from TIG-3 on fibronectin-coated dish and sub-cultured on fibronectin-coated dishes with hESF9 medium at passage 2. Bars indicate 200 μm.
(TIF)

Figure S3 Transduction Efficiency of Retroviruses in Dental Pulp cells. DPCs were introduced with pMXs retroviruses containing the EGFP cDNA. After 4 days, cells were photographed under a fluorescence microscope and analyzed by flow cytometry. The upper panel shows the images of phase contrast and fluorescent microscope. The lower panel shows the result of flow cytometry. Shown are percentages of cells expressing GFP. Transfection efficiency of EGFP was 92.1% in serum-supplemented condition and 89.9% in serum-free culture condition of transfected cells. Bars indicate 200 μm.
(TIF)

Figure S4 hiPS cell generation from DPCs in serum- and feeder-free culture conditions. Images of DPCs (DP-F) plated on collagen-coated dish in RD6F medium. A) Images of DPCs (passage 2) on type I collagen-coated plate with RD6F medium. B) Transduced DPCs were cultured on fibronectin with hESF9 medium or on MEF with KSR-based conditions. After 20 days, iPS colony were picked up and sub-cultured on fibronectin. The reprogramming efficiency was 0.25% with a high success rate. C) ALP staining of iPSCs on fibronectin at 33 days after infection. Bars indicate 200 μm.
(TIF)

Figure S5 Global gene expression analysis of hiPSCs from DPCs. The gene expression of DP-hiPSCs generated in hESF9 and maintained in hESF9T is similar to that of the cells generated and maintained in conventional KSR-based condition or that of Tic (JCRB1331) maintained in conventional KSR-based condition.
(TIF)

Figure S6 karyotype of hiPSC generated in hESF9 and maintained in hESF9T defined culture. A) Growth curve of hiPSCs. Shown were averages. Growth curves for the hiPSC (DP-F-iPS-CL16) cultured under hESF9T at passage 21, 22, 23 and 24 were seeded in a 24-well plate coated with fibronectin and the cell numbers were counted every 24 h. The values are the mean± SEM (n = 4). Population doubling time: 16.6±0.843 h. B) Karyotype analysis of DP-F-iPS-CL14 cell at passage 20 maintained in hESF9T conditions. Normal diploid 46, XX karyotype.
(TIF)

Table S1 Composition of medium used for serum-free culture. The composition of the basal medium RD is described in Sato, JD et al., 1987[11]. hESF9 medium is described in Furue et al., 2008 [5].
(TIF)

Table S2 Primers used in this study listed.
(TIF)

Table S3 STR analyses of DP-derived iPSCs.
(TIF)

Acknowledgments

We thank Dr. J. Denry Sato for editorial assistance. The authors are grateful to Dr. Miho K. Furue at NIBIO for valuable suggestions. We are also grateful to Ms. Michiko Nii, Atsuko Hamada and Eri Akagi at Hiroshima University for karyotype analysis of the hiPSCs.

Author Contributions

Conceived and designed the experiments: SY AS TO. Performed the experiments: SY YT HM. Analyzed the data: SY AS TO. Contributed reagents/materials/analysis tools: AS HT TO. Wrote the paper: SY TO.

References

1. Takahashi K, Tanabe K, Ohnuki M, Narita M, Ichisaka T, et al. (2007) Induction of pluripotent stem cells from adult human fibroblasts by defined factors. Cell 131: 861–872.
2. Yu J, Vodyanik MA, Smuga-Otto K, Antosiewicz-Bourget J, Frane JL, et al. (2007) Induced pluripotent stem cell lines derived from human somatic cells. Science 318: 1917–1920.
3. Hayashi Y, Chan T, Warashima M, Fukuda M, Ariizumi T, et al. (2010) Reduction of N-Glycolylneuraminic Acid in Human Induced Pluripotent Stem Cells Generation or Cultured under Feeder-and Serum-Free Defined Condition. PLoS One 5: e14099.
4. Chen G, Gulbranson DR, Hou Z, Bolin JM, Ruotti V, et al. (2011) Chemically defined conditions for human iPSC derivation and culture. Nat Methods 8: 424–429.
5. Furue MK, Na J, Jackson JP, Okamoto T, Jones M, et al. (2008) Heparin promotes the growth of human embryonic stem cells in a defined serum-free medium. Proc Natl Acad Sci USA 105: 13409–13414.
6. Morita S, Kojima T, Kitamura T (2000) Plat-E: an efficient and stable system for transient packaging of retroviruses. Gene Ther 7:1063–1066.
7. Matsuo M, Kaji K, Utakoji T, Hosoda K (1982) Ploidy of human embryonic fibroblasts during in vitro aging. J Gerontol 37: 33–37.
8. Takahashi K, Okita K, Nakagawa M, Yamanaka S (2007) Induction of pluripotent stem cells from fibroblast cultures. Nat Protoc 2:3081–3089.
9. Draper JS, Moore HD, Ruban LN, Gokhale PJ, Andrews PW (2004) Culture and characterization of human embryonic stem cells. Stem Cells Dev 13: 325–36.
10. Park IH, Zhao R, West JA, Yabuuchi A, Huo H, et al. (2008) Reprogramming of human somatic cells to pluripotency with defined factors. Nature 451:141–146.
11. Sato JD, Kawamoto T, Okamoto T (1987) Cholesterol requirement of P3-X63-Ag8 and X63-Ag8.653 mouse myeloma cells for growth in vitro. J Exp Med 165:1761–1766.
12. Myoken Y, Okamoto T, Osaki T, Yabumoto M, Sato GH, et al. (1989) An alternative method for the isolation of NS-1 hybridomas using cholesterol auxotrophy of NS-1 mouse myeloma cells. In Vitro Cell Dev Biol 25: 477–480.
13. Furue M, Okamoto T, Hayashi Y, Okochi H, Fujimoto M, et al. (2005) Leukemia inhibitory factor as anti-apoptotic mitogen for pluripotent mouse embryonic stem cells in a serum-free medium without feeder cells. In Vitro Cell Dev Biol Anim 41: 19–28.
14. Rajala K, Hakala H, Panula S, Aivio S, Pihlajamäki H, et al. (2007) Testing of nine different xenofree culture media for human embryonic stem cell cultures. Hum Reprod 22:1231–1238.
15. Gu J, Fujibayashi A, Yamada KM, Sekiguchi K (2002) Laminin-10/11 and fibronectin differentially prevent apoptosis induced by serum removal via phosphatidylinositol 3-kinase/Akt- and MEK1/ERK-dependent pathways. J Biol Chem 277:19922–19928.
16. Braam SR, Zeinstra L, Litjens S, Ward-van Oostwaard D, van den Brink S, et al. (2008) Recombinant vitronectin is a functionally defined substrate that supports human embryonic stem cell self-renewal via alphavbeta5 integrin. Stem Cells 26: 2257–2265.
17. Prowse AB, Doran MR, Cooper-White JJ, Chong F, Munro TP, et al. (2010) Long term culture of human embryonic stem cells on recombinant vitronectin in ascorbate free media. Biomaterials 31: 8281–8288.
18. Lu J, Hou R, Booth CJ, Yang SH, Snyder M (2006) Defined culture conditions of human embryonic stem cells. Proc. Natl Acad. Sci. USA 103: 5688–5693.
19. Rodin S, Domogatskaya A, Ström S, Hansson EM, Chien KR, et al. (2010) Long-term self-renewal of human pluripotent stem cells on human pluripotent stem cells on human recombinant laminin-511. Nat biotechnol 28: 611–615.
20. Miyazaki T, Futaki S, Suemori H, Taniguchi Y, Yamada M, et al. (2012) Laminin E8 fragments support efficient adhesion and expansion of dissociated human pluripotent stem cells. Nat Commun 3:1236.
21. Bendall SC, Stewart MH, Menendez P, George D, Vijayaragavan K, et al. (2007) IGF and FGF cooperatively establish the regulatory stem cell niche of pluripotent human cells in vitro. Nature 488:1015–1021.
22. Kunath T, Saba-El-Leil MK, Almousailleakh M, Wray J, Meloche S, et al. (2007) FGF stimulation of the Erk1/2 signaling cascade triggers transition of pluripotent embryonic stem cells from self-renewal to lineage commitment. Development 134:2895–2902.
23. Beattie GM, Lopez AD, Bucay N, Hinton A, Firpo MT, et al. (2005) Activin A maintains pluripotency of human embryonic stem cells in the absence of feeder layers. Stem Cells 23:489–495.
24. James D, Levine AJ, Besser D, Hemmati-Brivanlou A (2005) TGFbeta/activin/nodal signaling is necessary for the maintenance of pluripotency in human embryonic stem cells Development 132:1273–1282.
25. Xiao L, Yuan X, Sharkis SJ (2006) Activin A maintains self-renewal and regulates fibroblast growth factor, Wnt, and bone morphogenic protein pathways in human embryonic stem cells. Stem Cells 24:1476–1486.
26. Xu RH, Sampsell-Barron TL, Gu F, Root S, Peck RM, et al. (2008) NANOG is a direct target of TGF beta/activin-mediated SMAD signaling in human ESCs. Cell Stem Cell 3:196–206.
27. Vallier L, Mendjan S, Brown S, Chng Z, Teo A, et al. (2009) Activin/Nodal signaling maintains pluripotency by controlling Nanog expression. Development 136: 1339–1349.
28. Singh AM, Reynolds D, Cliff T, Ohtsuka S, Mattheyses AL, et al. (2012) Signaling network crosstalk in human pluripotent cells: a Smad2/3-regulated switch that controls the balance between self-renewal and differentiation. Cell Stem Cell 10:312–326.
29. Li H, Xu D, Li J, Berndt MC, Liu JP (2006) Transforming growth factor beta suppresses human telomerase reverse transcriptase by Smad3 interactions with C-Myc and hTERT gene. J Biol Chem 35:25588–25600.
30. Tamaoki N, Takahashi K, Tanaka T, Ichisaka T, Aoki H, et al. (2010) Dental pulp cells for induced pluripotent stem cell banking. J Dent Res 89:773-778.
31. Oda Y, Yoshimura Y, Ohnishi H, Tadokoro M, Katsube Y, et al. (2010) Induction of pluripotent stem cells from human third molar mesenchymal stromal cells. J Biol Chem 285: 29270–29278.
32. Yan X, Qin H, Qu C, Tuan RS, Shi S, et al. (2010) iPS cells reprogrammed from human mesenchymal-like stem/progenitor cells of dental tissue origin. Stem Cells Dev 19:469–480.
33. Okita K, Nakagawa M, Hyenjong H, Ichisaka T, Yamanaka S (2008) Generation of mouse induced pluripotent stem cells without viral vectors. Science 322:949–953.
34. Stadtfeld M, Nagaya M, Utikal J, Weir G, Hochedlinger K (2008) Induced pluripotent stem cells generated without viral integration. Science 322:945–949.
35. Yu J, Hu K, Smuga-Otto K, Tian S, Stewart R, et al. (2009) Human induced pluripotent stem cells free of vector and transgene sequences. Science 324:797–801.
36. Zhu S, Li W, Zhou H, Wei W, Ambasudhan R, et al. (2010) Reprogramming of human primary somatic cells by OCT4 and chemical compounds. Cell Stem Cell 7:651–655.
37. Kim D, Kim CH, Moon JI, Chung YG, Chang MY, et al. (2009) Generation of human induced pluripotent stem cells by direct delivery of reprogramming proteins. Cell Stem Cell 4:472–476.
38. Miyoshi N, Ishii H, Nagano H, Haraguchi N, Dewi DL, et al. (2011) Reprogramming of mouse and human cells to pluripotency using mature microRNAs. Cell Stem Cell 8:633–638.
39. Nakagawa M, Koyanagi M, Tanabe K, Takahashi K, Ichisaka T, et al. (2008) Generation of Induced Pluripotent Stem Cells without Myc from mouse and human fibroblasts. Nat Biotechnol 26:101–106.
40. Nakagawa M, Takizawa N, Narita M, Ichisaka T, Yamanaka S (2010) Promotion of direct reprogramming by transfection-deficient myc. Proc Natl Acad Sci U S A 107:14152–14157.

Cell Reports
Article

Two Distinct Modes of ATR Activation Orchestrated by Rad17 and Nbs1

Bunsyo Shiotani,[1,3,*] Hai Dang Nguyen,[1] Pelle Håkansson,[1,4] Alexandre Maréchal,[1] Alice Tse,[1] Hidetoshi Tahara,[3] and Lee Zou[1,2,*]

[1]Massachusetts General Hospital Cancer Center, Harvard Medical School, Charlestown, MA 02129, USA
[2]Department of Pathology, Massachusetts General Hospital and Harvard Medical School, Boston, MA 02114, USA
[3]Department of Cellular and Molecular Biology, Hiroshima University, Hiroshima 734-8553, Japan
[4]Present address: Department of Medical Biochemistry and Biophysics, Umeå University, SE-90187 Umeå, Sweden
*Correspondence: bshiotan@hiroshima-u.ac.jp (B.S.), zou.lee@mgh.harvard.edu (L.Z.)
http://dx.doi.org/10.1016/j.celrep.2013.04.018

SUMMARY

The ATM- and Rad3-related (ATR) kinase is a master regulator of the DNA damage response, yet how ATR is activated toward different substrates is still poorly understood. Here, we show that ATR phosphorylates Chk1 and RPA32 through distinct mechanisms at replication-associated DNA double-stranded breaks (DSBs). In contrast to the rapid phosphorylation of Chk1, RPA32 is progressively phosphorylated by ATR at Ser33 during DSB resection prior to the phosphorylation of Ser4/Ser8 by DNA-PKcs. Surprisingly, despite its reliance on ATR and TopBP1, substantial RPA32 Ser33 phosphorylation occurs in a Rad17-independent but Nbs1-dependent manner in vivo and in vitro. Importantly, the role of Nbs1 in RPA32 phosphorylation can be separated from ATM activation and DSB resection, and it is dependent upon the interaction of Nbs1 with RPA. An Nbs1 mutant that is unable to bind RPA fails to support proper recovery of collapsed replication forks, suggesting that the Nbs1-mediated mode of ATR activation is important for the repair of replication-associated DSBs.

INTRODUCTION

The ability of cells to sense and signal DNA damage in their genomes is crucial for genomic stability. In human cells, the *ataxia telangiectasia* mutated (ATM) and the ATM- and Rad3-related (ATR) kinases are two master regulators of DNA damage signaling (Ciccia and Elledge, 2010). ATM, ATR, and their related DNA-dependent protein kinase catalytic subunit (DNA-PKcs) belong to the PI3K-like kinase (PIKK) family. Whereas ATM and DNA-PKcs are primarily activated by DNA double-stranded breaks (DSBs), ATR responds to a broad spectrum of DNA damage (Cimprich and Cortez, 2008; Flynn and Zou, 2011). Unlike ATM and DNA-PKcs, ATR is essential for cell survival even in the absence of extrinsic DNA damage, underscoring the critical function of ATR in coping with intrinsic genomic stress (Barlow et al., 2013; Brown and Baltimore, 2000; Murga et al., 2009; Toledo et al., 2011). Although the DNA-damage specificities and functions of ATM, ATR, and DNA-PKcs are clearly distinct, how they distinguish different types of DNA damage and execute their unique functions is still poorly understood. In particular, it is largely unknown how ATR is activated by different types of DNA damage and replication stress.

Studies in different organisms have revealed some of the key principles of ATR activation. In response to DNA damage and replication stress, the complex of ATR and its functional partner, ATR-interacting protein (ATRIP), is recruited to sites of DNA damage and stalled replication forks by replication protein A (RPA)-coated single-stranded DNA (RPA-ssDNA) (Byun et al., 2005; Costanzo et al., 2003; Zou and Elledge, 2003). The activation of ATR-ATRIP requires additional regulators, such as the Rad17-RFC complex, the Rad9-Rad1-Hus1 (9-1-1) complex, and TopBP1 (Kumagai et al., 2006; Lin et al., 2012; Navadgi-Patil and Burgers, 2009; Zou et al., 2002). Independently of the recruitment of ATR-ATRIP to RPA-ssDNA, the Rad17-RFC complex recognizes the junctions of ssDNA and double-stranded DNA (dsDNA) and loads 9-1-1 complexes onto dsDNA (Ellison and Stillman, 2003; Zou et al., 2003). Through a process that is still not fully understood, TopBP1 is recruited to damaged DNA and interacts with Rad17, 9-1-1, and autophosphorylated ATR (Cotta-Ramusino et al., 2011; Delacroix et al., 2007; Lee and Dunphy, 2010; Lee et al., 2007; Liu et al., 2011; Wang et al., 2011; Yan and Michael, 2009). The engagement of TopBP1 with ATR-ATRIP allows TopBP1 to stimulate the kinase activity of ATR and to facilitate ATR to recognize its substrates (Kumagai et al., 2006; Liu et al., 2011; Mordes et al., 2008). In this model of ATR activation, ATR is activated by Rad17 and TopBP1 around ssDNA/dsDNA junctions. Indeed, checkpoint kinase 1 (Chk1), an effector kinase of ATR that is critical for the replication stress response and cell-cycle arrest, is phosphorylated by ATR in a Rad17-, TopBP1-, and ssDNA/dsDNA-junction-dependent manner (Liu et al., 2006; MacDougall et al., 2007; Van et al., 2010; Yamane et al., 2003; Zou et al., 2002). However, it is important to note that although Chk1 phosphorylation has been widely used as a surrogate for ATR activation, it remains unclear whether Chk1 phosphorylation accurately evinces the active mode of ATR in all situations.

In this study, we asked whether ATR is always activated by the Rad17-TopBP1 circuitry after DNA damage occurs. In particular, we wondered whether ATR is activated by Rad17 and TopBP1 at extensively resected DSBs, such as those generated in S phase

Cell PRESS
Open ACCESS

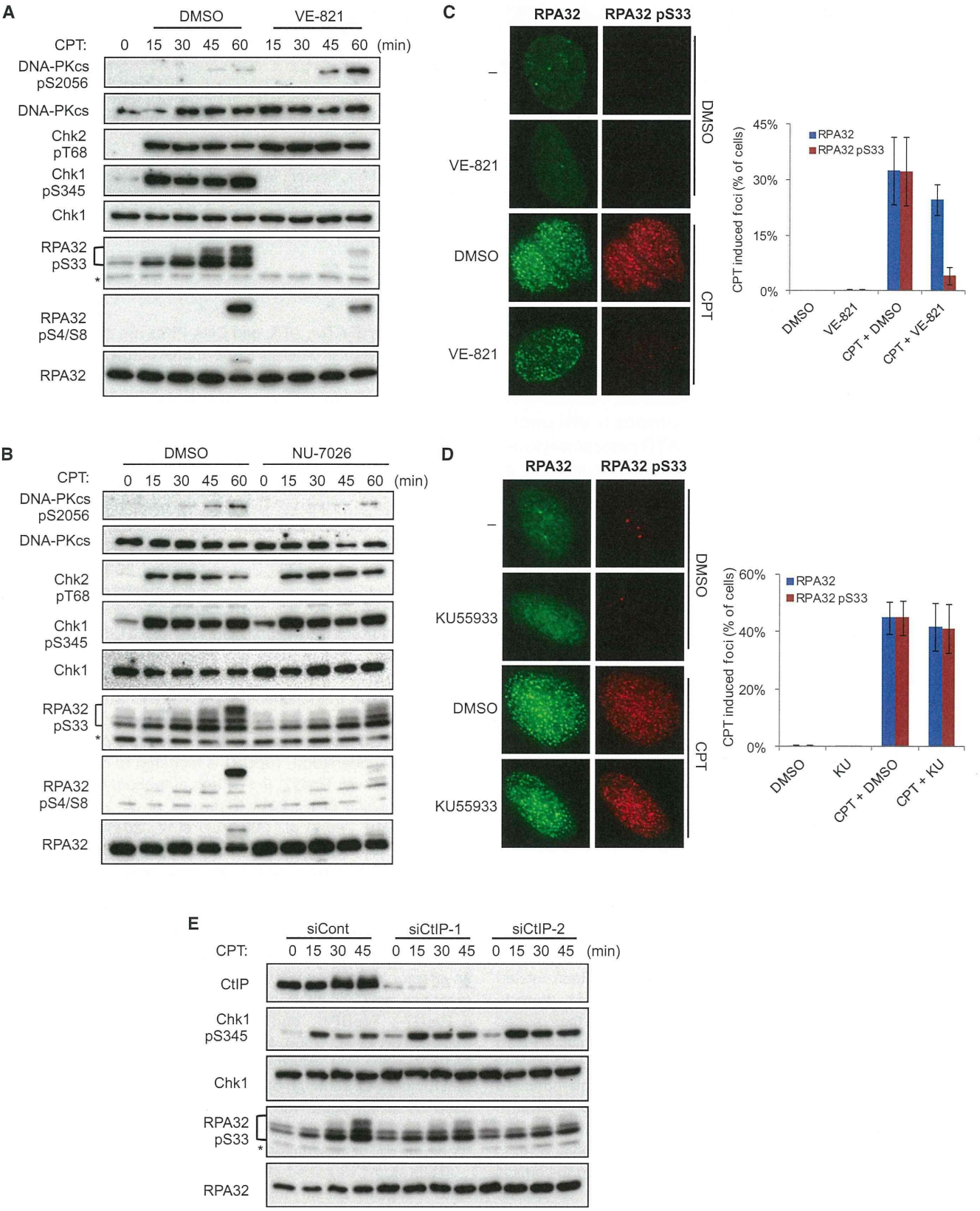

(legend on next page)

at collapsed replication forks. When long ssDNA is generated at DSBs by resection, a fraction of ATR could be recruited to the RPA-ssDNA distal to ssDNA/dsDNA junctions, raising the question as to whether and how this fraction of ATR is activated on RPA-ssDNA. To address this question, we analyzed the activation of ATR by camptothecin (CPT), which induces replication-associated DSBs that undergo rapid and efficient resection (Avemann et al., 1988; Sartori et al., 2007). We found that ATR is activated in two distinct modes toward Chk1 and RPA32. In one mode, ATR phosphorylates Chk1 rapidly, whereas in the other mode, ATR phosphorylates RPA32 Ser33 progressively during resection. The activation of ATR toward RPA32 is driven by resection and requires TopBP1. Surprisingly, Nbs1, a component of the Mre1-Rad50-Nbs1 (MRN) complex (Carney et al., 1998; Costanzo et al., 2001; Difilippantonio et al., 2005; Stracker and Petrini, 2011), plays a more important role than Rad17 in the phosphorylation of RPA32. The function of Nbs1 in RPA32 phosphorylation can be separated from ATM activation and DSB resection, and is dependent upon a direct interaction between Nbs1 and RPA. An Nbs1 mutant that is unable to bind RPA is compromised in its ability to support the recovery of collapsed replication forks. Together, these results suggest that Nbs1 mediates a TopBP1-dependent but Rad17-independent mode of ATR activation on RPA-ssDNA, allowing ATR to phosphorylate substrates such as RPA32 independently of ssDNA/dsDNA junctions and promote repair of replication-associated DSBs.

RESULTS

ATR Phosphorylates Chk1 and RPA32 Ser33 via Distinct Mechanisms

ATR is known to be activated by the replication-associated DSBs induced by CPT (Avemann et al., 1988; Sartori et al., 2007). Using VE-821, a specific ATR inhibitor (Reaper et al., 2011), we confirmed that a number of ATR substrates, including Chk1, Rad17, RPA32, and ATR itself, were phosphorylated in an ATR-dependent manner after CPT treatment (Figure S1A). In contrast to these ATR substrates, ATM and DNA-PKcs underwent efficient autophosphorylation in the presence of VE-821 (Figure S1B). Furthermore, the phosphorylation of several ATM and/or DNA-PKcs substrates, including Chk2, p53, and H2AX, was not affected by VE-821 (Figure S1B). These results confirm that VE-821 specifically inhibits ATR, but not ATM and DNA-PKcs, in CPT-treated cells.

In response to CPT, RPA32 is phosphorylated at multiple sites, including Ser4/Ser8, Thr21, and Ser33 (Anantha et al., 2007; Block et al., 2004; Sartori et al., 2007). Using phosphospecific antibodies, we found that RPA32 Ser33 was phosphorylated within 15 min after CPT treatment, whereas RPA32 Ser4/Ser8 was phosphorylated at ~60 min (Figure 1A). Furthermore, the phosphorylation of RPA32 Ser33 was abolished by VE-821, whereas RPA32 Ser4/Ser8 phosphorylation was only partially reduced (Figure 1A). The phosphorylation of RPA32 Ser4/Ser8 was shown to be DNA-PKcs dependent (Anantha et al., 2007; Liaw et al., 2011; Liu et al., 2012). Indeed, the CPT-induced phosphorylation of RPA32 Ser4/Ser8 was abolished by the DNA-PKcs inhibitor NU7026 (Figure 1B). In contrast, RPA32 Ser33 phosphorylation was not affected by NU7026 (Figure 1B). Thus, compared with the phosphorylation of RPA32 Ser4/Ser8, the phosphorylation of RPA32 Ser33 is a more direct and reliable marker for ATR activation.

The phosphorylation of RPA32 has been linked to DSB resection (Sartori et al., 2007). A recent study suggested that ATR promotes resection in *Xenopus* extracts (Peterson et al., 2013). Consistent with this finding, at 1 hr after CPT treatment, the formation of RPA32 foci was reduced by VE-821 (Figure 1C). Nevertheless, a significant fraction of VE-821-treated cells displayed RPA32 foci, suggesting that ATR is not essential for resection (Figure 1C). Importantly, the majority of VE-821-treated cells that displayed RPA32 foci were negative for phospho-Ser33 foci, suggesting that ATR is required for RPA32 Ser33 phosphorylation after resection (Figure 1C). In contrast to VE-821, the ATM inhibitor KU55933 drastically diminished the foci of both RPA32 and phospho-Ser33 1 hr after CPT treatment (Figure S1C). At 2 hr, KU55933-treated cells no longer displayed a significant reduction in RPA32 foci and phospho-Ser33 foci (Figure 1D), showing that inhibition of ATM delays resection transiently. In KU55933-treated cells, RPA32 foci were always colocalized with phospho-Ser33 foci (Figure 1D), suggesting that ATM does not have a direct role in RPA32 Ser33 phosphorylation post resection. Consistent with RPA32 Ser33 phosphorylation being a specific marker of ATR activation, this phosphorylation event was clearly detected in the ATM-deficient AT cells and the DNA-PKcs-deficient M059J cells, even when they were treated with NU7026 and KU55933, respectively (Figures S1D and S1E).

Having established RPA32 Ser33 phosphorylation as a marker for CPT-induced ATR activation, we asked whether this phosphorylation event is regulated in the same way as Chk1 phosphorylation. In response to CPT, Chk1 was rapidly phosphorylated at Ser345 in an ATR-dependent manner (Figure 1A). In contrast to the phosphorylation of RPA32 Ser33, which

Figure 1. ATR-Mediated RPA32 Ser33 Phosphorylation in Response to CPT-Induced DSBs

(A) U2OS cells were treated with 1 μM CPT in the presence or absence of 10 μM VE-821 and collected at the indicated times. The levels of the indicated proteins and the CPT-induced phosphorylation events were analyzed by western blot; *a protein cross-reacting to the phospho-Ser33 antibody.

(B) Cells pretreated with 10 μM NU-7026 or DMSO for 1 hr were exposed to 1 μM CPT in the presence or absence of 10 μM NU-7026. Extracts were analyzed as in (A).

(C) Cells were treated with 1 μM CPT for 1 hr, or mock treated, in the absence or presence of VE-821. Immunofluorescence analysis of RPA32 and phospho-Ser33 was performed with specific antibodies. Representative images of cells are shown in the left panel. The fractions of cells that displayed RPA32 or phospho-Ser33 foci are shown in the right panel. Error bars: SDs from three independent experiments (n = 3).

(D) Cells were treated with 1 μM CPT for 2 hr, or mock treated, in the absence or presence of KU55933. Immunofluorescence analysis was performed and quantified as in (C). Error bars: SDs from three independent experiments (n = 3).

(E) U2OS cells transfected with control or CtIP siRNAs were treated with 1 μM CPT and collected at the indicated time points. Extracts were analyzed as in (A). See also Figure S1.

Cell PRESS
Open ACCESS

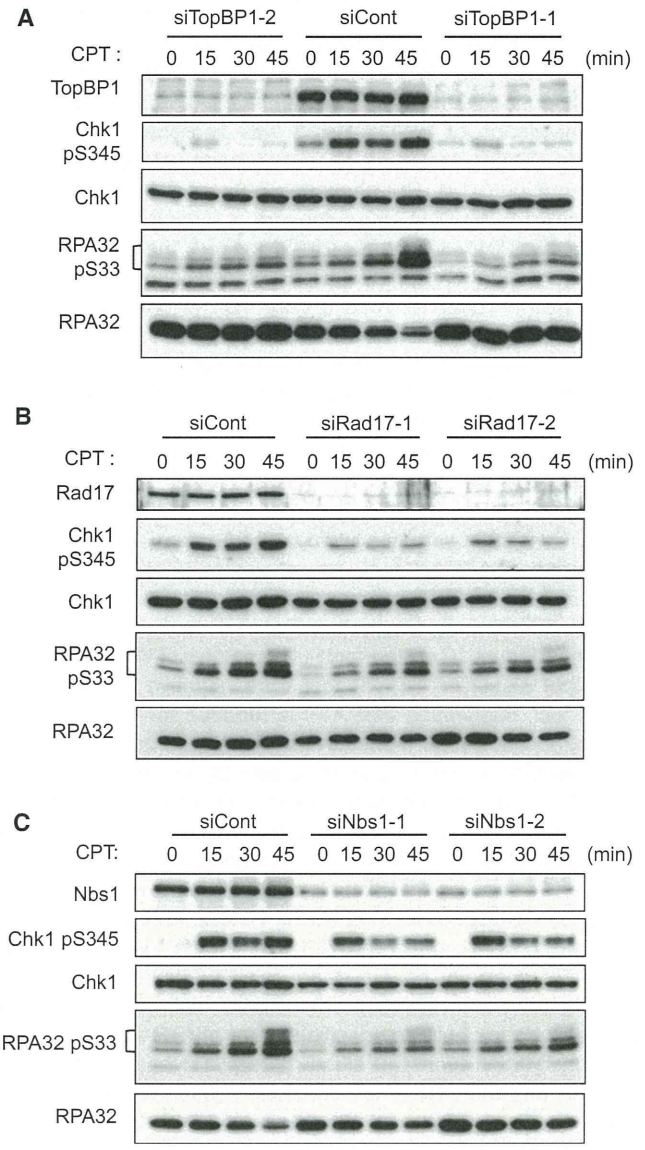

Figure 2. RPA32 and Chk1 Are Phosphorylated by ATR through Distinct Mechanisms

(A–C) U2OS cells transfected with control, TopBP1 (A), Rad17 (B), or Nbs1 (C) siRNAs were treated with 1 μM CPT and collected at the indicated time points. The levels of the indicated proteins and the CPT-induced phosphorylation events were analyzed by western blot.

See also Figure S2.

gradually accumulated during the first 60 min after CPT treatment, Chk1 phosphorylation plateaued within 15 min (Figure 1A). Thus, Chk1 and RPA32 Ser33 are phosphorylated by ATR with distinct kinetics. Consistent with the sequential phosphorylation of RPA32 by ATR and DNA-PKcs (Anantha et al., 2007), the phosphorylation of RPA32 Ser4/Ser8 by DNA-PKcs occurred significantly later than Ser33 phosphorylation and Chk1 phosphorylation (Figure 1A; Kousholt et al., 2012).

The phosphorylation of RPA32 Ser4/Ser8 by DNA-PKcs requires CtIP, which is critical for resection (Sartori et al., 2007). Prior to the abrupt phosphorylation of Ser4/Ser8, Ser33 was gradually phosphorylated by ATR (Figure 1A), suggesting that Ser33 phosphorylation may be the initial phosphorylation event on RPA32 that is driven by resection. Indeed, knockdown of CtIP with two independent small interfering RNAs (siRNAs) drastically reduced the phosphorylation of RPA32 Ser33 during the first 45 min after CPT treatment (Figure 1E). On the other hand, consistent with a recent report (Kousholt et al., 2012), depletion of CtIP did not significantly affect the phosphorylation of Chk1 during this early phase of the CPT response. Thus, in contrast to the rapid phosphorylation of Chk1, the phosphorylation of RPA32 Ser33 by ATR occurs progressively during resection.

Distinct Roles of Rad17 and Nbs1 in RPA Phosphorylation

The distinct kinetics and resection dependency of Chk1 and RPA32 phosphorylation prompted us to investigate whether ATR is activated toward these two substrates in different ways. To dissect the genetic requirements for RPA32 Ser33 phosphorylation, we used siRNAs to knock down the upstream regulators of the ATR pathway. Consistent with the effects of VE-821, knockdown of ATR abolished the phosphorylation of both Chk1 and RPA32 Ser33 (Figure S2A). Two independent siRNAs targeting TopBP1, the key activator of ATR, also drastically reduced the phosphorylation of Chk1 and RPA32 Ser33 (Figure 2A). Therefore, similar to Chk1 phosphorylation, RPA32 Ser33 phosphorylation requires both ATR and TopBP1.

TopBP1 and Rad17 function together in Chk1 phosphorylation (Delacroix et al., 2007; Lee and Dunphy, 2010). As expected, knockdown of Rad17 with two independent siRNAs significantly reduced Chk1 phosphorylation (Figure 2B). Surprisingly, however, substantial RPA32 Ser33 phosphorylation was detected in Rad17 knockdown cells (Figure 2B), suggesting the existence of a Rad17-independent mechanism of RPA32 Ser33 phosphorylation. The MRN complex has been implicated in ATR regulation and RPA phosphorylation (Jazayeri et al., 2006; Manthey et al., 2007; Myers and Cortez, 2006; Olson et al., 2007a; Stiff et al., 2005; Yoo et al., 2009; Zhong et al., 2005). Knockdown of Nbs1 with two independent siRNAs clearly reduced RPA32 Ser33 phosphorylation without altering cell-cycle distribution (Figures 2C and S2B). Consistent with Nbs1 knockdown, the Nbs1-deficient NBN-ILB1 cells displayed much lower RPA32 Ser33 phosphorylation than the Nbs1-complemented cells (Figure S2C). Compared with Rad17 knockdown, Nbs1 knockdown reduced RPA32 Ser33 phosphorylation to a greater extent. When both Rad17 and Nbs1 were knocked down, RPA32 Ser33 phosphorylation was further reduced (Figure S2D), suggesting that Rad17 and Nbs1 function in parallel to activate ATR toward RPA32 Ser33. Interestingly, although Nbs1 knockdown clearly reduced RPA32 Ser33 phosphorylation, its effects on Chk1 phosphorylation were modest (Figure 2C). Thus, in contrast to Rad17, Nbs1 plays a more important role in RPA phosphorylation than in Chk1 phosphorylation.

Nbs1 Mediates RPA32 Phosphorylation Independently of Rad17 and ssDNA/dsDNA Junctions

The MRN complex regulates ATM activation and DSB resection (Symington and Gautier, 2011; Uziel et al., 2003). Furthermore,

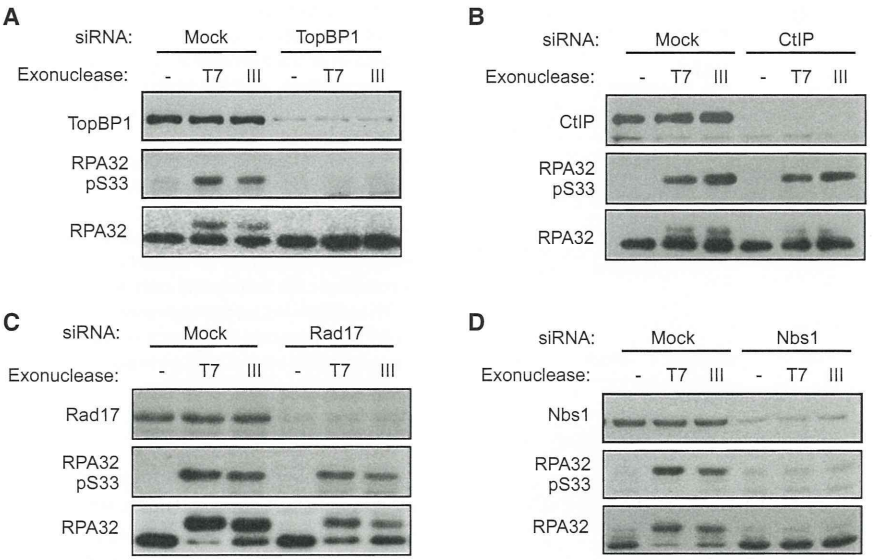

Figure 3. Nbs1 Regulates RPA32 Phosphorylation Independently of ATM Activation and DSB Resection

(A) Nuclear extracts were prepared from HeLa cells transfected with TopBP1 siRNA or mock transfected. A 6 kb dsDNA fragment was resected with T7 exonuclease or exonuclease III as described in the Experimental Procedures. Resected or unresected dsDNA was added to cell extracts, and the resected-dsDNA-induced phosphorylation of RPA32 Ser33 was analyzed with phosphospecific antibody.

(B) The resected-dsDNA-induced phosphorylation of RPA32 Ser33 was analyzed in extracts of CtIP knockdown cells and control cells as in (A).

(C) The resected-dsDNA-induced phosphorylation of RPA32 Ser33 was analyzed in extracts of Rad17 knockdown cells and control cells as in (A).

(D) The resected-dsDNA-induced phosphorylation of RPA32 Ser33 was analyzed in extracts of Nbs1 knockdown cells and control cells as in (A).

the MRN complex is implicated in the removal of TopI from CPT-induced DSBs (Sacho and Maizels, 2011). To determine whether Nbs1 regulates RPA32 phosphorylation directly or indirectly, we analyzed the function of Nbs1 in RPA32 phosphorylation using an in vitro assay that we recently developed (Shiotani and Zou, 2009). In this assay, linear dsDNA is resected by T7 exonuclease or exonuclease III to generate ssDNA overhangs, and subsequently is added to HeLa cell nuclear extracts to activate ATR (Shiotani and Zou, 2011). Using this assay, we have shown that RPA32 Ser33 is phosphorylated in an ATR-dependent manner. Since both ATM and DNA-PKcs are inhibited in extracts, and dsDNA is already resected before it is added to extracts, this assay provides a unique opportunity to test whether Nbs1 has an ATM-, resection-, and end-processing-independent function in RPA32 phosphorylation.

Consistent with its dependency on TopBP1 in cells, RPA32 Ser33 phosphorylation was not induced by resected dsDNA in extracts derived from TopBP1 knockdown cells (Figure 3A). In contrast, RPA32 Ser33 phosphorylation occurred efficiently in extracts from CtIP knockdown cells, confirming that the role of MRN-CtIP in DSB resection is bypassed by the use of preresected dsDNA in this assay (Figure 3B). Also consistent with the observation in cells, the phosphorylation of RPA32 Ser33 in extracts was only modestly reduced by Rad17 depletion (Figure 3C). Strikingly, even in this resection-independent in vitro assay, Nbs1 was clearly required for RPA32 Ser33 phosphorylation (Figure 3D). These results reveal a postresection function of Nbs1 in RPA32 phosphorylation.

Since substantial RPA32 Ser33 phosphorylation occurred independently of Rad17 in vivo and in vitro, we asked if this phosphorylation event is absolutely dependent upon ssDNA/dsDNA junctions. In nuclear extracts, ssDNA alone was sufficient to induce RPA32 Ser33 phosphorylation in a length-dependent manner (Figure 4A). We noted that unlike resected dsDNA, ssDNA did not induce a mobility shift of RPA32 in protein gels. The reason for this difference is currently unknown. Importantly, the ssDNA-induced RPA32 Ser33 phosphorylation was dependent upon ATR, TopBP1, and Nbs1 (Figures 4B–4D), suggesting that a process driven by ssDNA lengthening and mediated by Nbs1 and TopBP1 is able to activate ATR toward RPA independently of ssDNA/dsDNA junctions.

Nbs1 Targets the MRN Complex to RPA-ssDNA

We next asked how Nbs1 executes its postresection function in ATR activation. The MRN complex interacts with RPA (Oakley et al., 2009; Olson et al., 2007b). Consistent with previous studies, we found that in extracts, Mre11, Rad50, and Nbs1 all bound to ssDNA in an RPA-dependent manner (Figure 5A). The RPA complex containing the RPA70 t-11 mutant, whose N-terminal oligonucleotide/oligosaccharide-binding (OB) fold was disrupted by point mutations, was unable to recruit MRN to ssDNA (Figure 5B). Furthermore, purified MRN complex bound to ssDNA in an RPA-dependent manner, showing that MRN associates with RPA-ssDNA directly (Figure 5C). Even in the absence of Mre11 and Rad50, purified Nbs1 bound to ssDNA in an RPA-dependent manner, suggesting a direct interaction between Nbs1 and RPA-ssDNA (Figure 5D).

To determine whether the recruitment of MRN to RPA-ssDNA is dependent on Nbs1, we generated extracts from Nbs1 knockdown cells. Consistent with previous studies, loss of Nbs1 did not affect the levels of Mre11 and Rad50 (Figure 5E; Stewart et al., 1999). However, in extracts of Nbs1 knockdown cells, neither Mre11 nor Rad50 bound to RPA-ssDNA efficiently (Figure 5E). In contrast to Mre11 and Rad50, ATRIP still associated with RPA-ssDNA efficiently in the absence of Nbs1 (Figure 5E). Together, these results suggest that Nbs1 targets the MRN complex to RPA-ssDNA.

Nbs1 Binds RPA-ssDNA via a Previously Uncharacterized Domain

To determine whether the interaction between Nbs1 and RPA-ssDNA is important for the phosphorylation of RPA32 Ser33 by

Cell PRESS
Open ACCESS

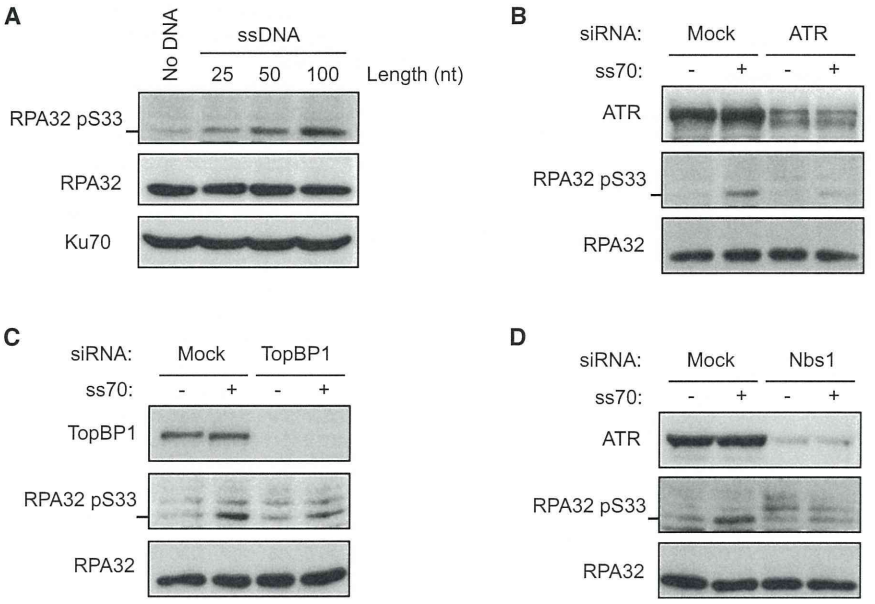

Figure 4. ssDNA Is Sufficient to Induce RPA32 Phosphorylation

(A) ssDNA of the indicated lengths was added to nuclear extracts, and the ssDNA-induced phosphorylation of RPA32 Ser33 was analyzed with phosphospecific antibody.

(B) The ssDNA-induced phosphorylation of RPA32 Ser33 was analyzed in extracts of ATR knockdown cells and control cells as in (A).

(C) The ssDNA-induced phosphorylation of RPA32 Ser33 was analyzed in extracts of TopBP1 knockdown cells and control cells as in (A).

(D) The ssDNA-induced phosphorylation of RPA32 Ser33 was analyzed in extracts of Nbs1 knockdown cells and control cells as in (A).

ATR, we sought to map the RPA-ssDNA-interacting domain of Nbs1. We expressed a set of myc-tagged Nbs1 fragments in cells and tested them for binding to biotinylated ssDNA coated with RPA (Figures 6A, S3A, and S3B). An Nbs1 fragment containing the N-terminal FHA and BRCT domains (Np38) was unable to interact with RPA-ssDNA (Figure S3A). On the other hand, two Nbs1 fragments lacking the FHA and BRCT domains (Cp49 and Cp38) retained the ability to interact with RPA-ssDNA (Figure S3B). Moreover, an Nbs1 fragment lacking the C-terminal ATM and Mre11 binding domains (Np75) still bound to RPA-ssDNA (Figure S3A). Thus, the RPA-ssDNA-interacting domain of Nbs1 is distinct from its known functional domains.

Through testing the binding of additional Nbs1 fragments to RPA-ssDNA (Figures S3A and S3B), we found that all of the Nbs1 fragments that were able to bind RPA-ssDNA encompassed amino acids 536–567 (Figure 6A). Alignment of the sequences of Nbs1 from different species revealed that a stretch of charged amino acids in this region is conserved in higher vertebrates (Figure 6B). To pinpoint the residues that are critical for RPA-ssDNA binding, we mutated the conserved residues KKR, DD, and EDE to EEG, AA, and AAA in full-length Nbs1, respectively (Figure 6B; Nbs1^{KKR}, Nbs1^{DD}, and Nbs1^{EDE}). Only the Nbs1^{EDE} mutant, and not the Nbs1^{KKR} and Nbs1^{DD} mutants, lost the ability to bind RPA-ssDNA (Figure 6C). The Nbs1^{EDE} mutant still bound to Mre11 efficiently (Figure 6D), suggesting that loss of the EDE motif of Nbs1 specifically disrupts its binding to RPA-ssDNA.

The Recognition of RPA-ssDNA by Nbs1 Is Important for RPA32 Ser33 Phosphorylation and Recovery of Collapsed Forks

To determine whether the binding of Nbs1 to RPA-ssDNA is important for RPA32 Ser33 phosphorylation, we first tested the Nbs1^{EDE} mutant in vitro. We expressed siRNA-resistant wild-type myc-Nbs1 (myc-Nbs1^{WT}) and myc-Nbs1^{EDE} in cells that were depleted of endogenous Nbs1 by siRNA and prepared extracts from these cells. In the myc-Nbs1^{WT}-containing extracts, resected dsDNA induced RPA32 Ser33 phosphorylation efficiently (Figure 7A). In contrast, RPA32 Ser33 phosphorylation was poorly induced by resected dsDNA in extracts containing myc-Nbs1^{EDE} (Figure 7A), suggesting that the ability of Nbs1 to recognize RPA-ssDNA is important for its postresection function in RPA32 Ser33 phosphorylation in vitro.

Next, we tested whether the Nbs1^{EDE} mutant is able to support RPA32 Ser33 phosphorylation in cells. We generated stable cell lines in which siRNA-resistant myc-Nbs1^{WT} or myc-Nbs1^{EDE} could be inducibly expressed. Upon induction of myc-Nbs1^{WT} in Nbs1 knockdown cells, RPA32 Ser33 phosphorylation was clearly induced by CPT (Figure 7B, lanes 3 and 4). In contrast, the levels of RPA32 Ser33 phosphorylation were not increased by CPT in cells expressing the myc-Nbs1^{EDE} mutant (Figure 7B, lanes 7 and 8). Thus, consistent with our in vitro experiments, the Nbs1^{EDE} mutant also fails to support RPA32 Ser33 phosphorylation in cells.

Finally, we sought to determine whether the recognition of RPA-ssDNA by Nbs1 is important for the DNA damage response. Because CPT induces replication-associated DSBs, we focused on the recovery of collapsed replication forks. We synchronized cells in S phase with thymidine and released them into CPT-containing media. As expected, γH2AX foci were induced in cells regardless of whether endogenous Nbs1 was replaced by myc-Nbs1^{WT} or myc-Nbs1^{EDE} (Figure 7C). After the myc-Nbs1^{WT}-expressing cells were released from CPT, γH2AX foci were largely gone in 24 hr (Figure 7C), indicating the recovery of collapsed forks. In contrast, a significant fraction of the myc-Nbs1^{EDE}-expressing cells retained γH2AX foci 24 hr after the release from CPT (Figure 7C), suggesting that the recovery of collapsed forks was compromised. These results establish a functional link between Nbs1-mediated ATR activation and the repair of replication-associated DSBs.

DISCUSSION

Many investigators have studied the activation of ATR using Chk1 phosphorylation as a readout. Both in vivo and in vitro

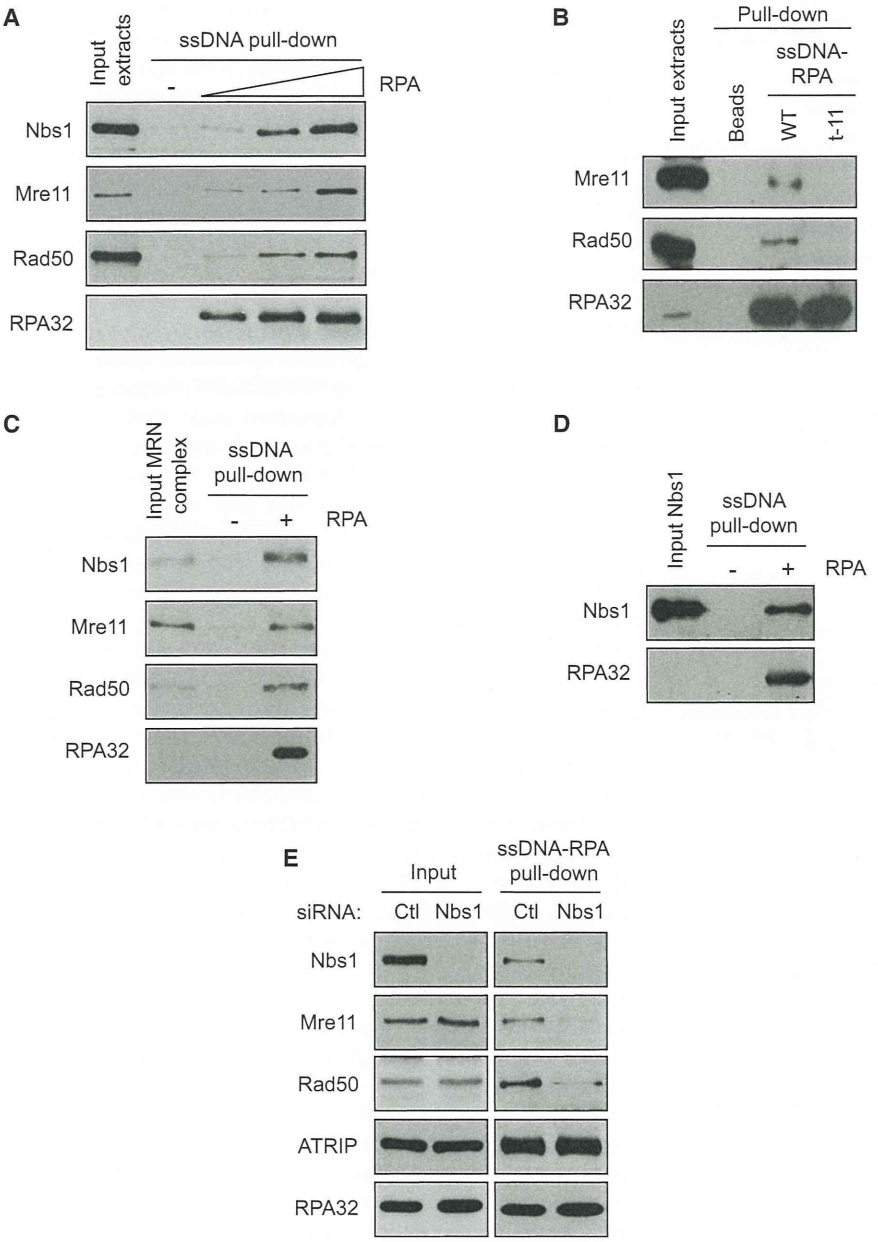

Figure 5. Nbs1 Targets the MRN Complex to RPA-ssDNA

(A) Biotinylated 70-nucleotide ssDNA (5 pmole) was coated with increasing amounts of purified RPA (0, 5, 10, and 20 pmole) and then incubated in cell extracts. The proteins bound to RPA-ssDNA were retrieved by streptavidin-coated beads and analyzed by western blot using the indicated antibodies. All components of the Mre11-Rad50-Nbs1 complex bound to ssDNA in an RPA-dependent manner.

(B) Biotinylated ssDNA was coated with either WT RPA or the RPA t-11 mutant complex purified from *E. coli*. The binding of Rad50 and Mre11 to RPA-ssDNA was tested as in (A).

(C) Biotinylated ssDNA coated with RPA was incubated with purified MRN complex. The MRN components bound to RPA-ssDNA were analyzed by western blot.

(D) Binding of purified Nbs1 to RPA-ssDNA was tested as in (C).

(E) Extracts were prepared from cells transfected with control or Nbs1-2 siRNA. Biotinylated ssDNA coated with RPA was incubated in the extracts, and the proteins bound to RPA-ssDNA were analyzed by western blot using the indicated antibodies.

experiments have suggested that Rad17 and TopBP1 are two key regulators of the activation of ATR toward Chk1 (Cimprich and Cortez, 2008; Flynn and Zou, 2011). In the current model of ATR activation, both RPA-ssDNA and ssDNA/dsDNA junctions are critical determinants of Chk1 phosphorylation (MacDougall et al., 2007). Whereas RPA-ssDNA presents a platform for ATR-ATRIP recruitment, the Rad17-RFC complex and 9-1-1 complexes are localized to ssDNA/dsDNA junctions. The co-localization of ATR-ATRIP, Rad17, 9-1-1, and TopBP1 around ssDNA/dsDNA junctions may create a protein-DNA assembly that allows TopBP1 to activate the ATR-ATRIP kinase complex and enable it to recognize its downstream substrates. This mechanism of ATR activation toward Chk1 is consistent with the fact that ssDNA is not sufficient to trigger checkpoint signaling through Chk1 (Guo and Dunphy, 2000; MacDougall et al., 2007).

Although ssDNA and ssDNA/dsDNA junctions are commonly induced by DNA damage and replication stress, the relative abundance of these two DNA structures may vary in different contexts. For example, at replication forks stalled by aphidicolin, an increased number of primers and ssDNA/dsDNA junctions may be generated, which would enhance the activation of ATR toward Chk1 (Van et al., 2010). On the other hand, when DSBs undergo extensive resection in S phase, long stretches of ssDNA may be generated without increasing the number of ssDNA/dsDNA junctions. We found that RPA32 Ser33 is progressively phosphorylated by ATR during the resection of CPT-induced DSBs. Although it is an ATR-mediated event, RPA32 Ser33 phosphorylation is regulated differently from Chk1 activation. In addition to its delayed kinetics and greater dependency on resection, RPA32 Ser33 phosphorylation is more dependent on Nbs1 but less dependent on Rad17 compared with Chk1 phosphorylation. Furthermore, unlike Chk1 phosphorylation, RPA32 Ser33 phosphorylation can occur on ssDNA in a length-dependent manner independently of ssDNA/dsDNA junctions. These findings suggest that, in a resection-driven manner, Nbs1 mediates a distinct mode of ATR activation toward RPA32.